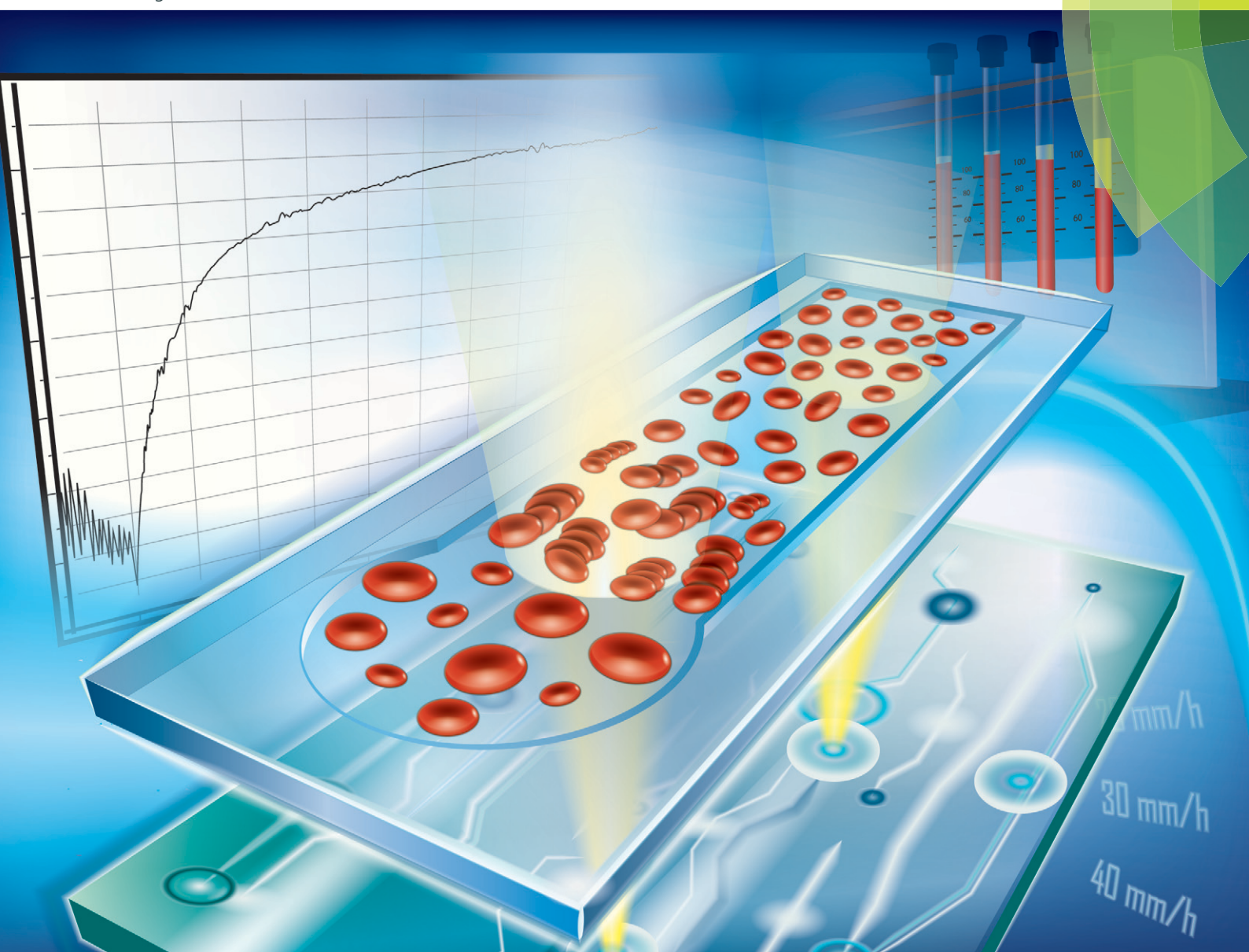


# Lab on a Chip

Miniaturisation for chemistry, physics, biology, materials science and bioengineering

[www.rsc.org/loc](http://www.rsc.org/loc)



ISSN 1473-0197



**PAPER**  
Caglar Elbuken *et al.*  
A portable microfluidic system for rapid measurement of the erythrocyte sedimentation rate

**175**  
YEARS



Cite this: *Lab Chip*, 2016, 16, 4682

## A portable microfluidic system for rapid measurement of the erythrocyte sedimentation rate

Ziya Isiksacan,<sup>a</sup> Ozcan Erel<sup>b</sup> and Caglar Elbuken<sup>\*a</sup>

The erythrocyte sedimentation rate (ESR) is a frequently used 30 min or 60 min clinical test for screening of several inflammatory conditions, infections, trauma, and malignant diseases, as well as non-inflammatory conditions including prostate cancer and stroke. Erythrocyte aggregation (EA) is a physiological process where erythrocytes form face-to-face linear structures, called rouleaux, at stasis or low shear rates. In this work, we proposed a method for ESR measurement from EA. We developed a microfluidic opto-electro-mechanical system, using which we experimentally showed a significant correlation ( $R^2 = 0.86$ ) between ESR and EA. The microfluidic system was shown to measure ESR from EA using fingerprick blood in 2 min. 40  $\mu\text{l}$  of whole blood is filled in a disposable polycarbonate cartridge which is illuminated with a near infrared emitting diode. Erythrocytes were disaggregated under the effect of a mechanical shear force using a solenoid pinch valve. Following complete disaggregation, transmitted light through the cartridge was measured using a photodetector for 1.5 min. The intensity level is at its lowest at complete disaggregation and highest at complete aggregation. We calculated ESR from the transmitted signal profile. We also developed another microfluidic cartridge specifically for monitoring the EA process in real-time during ESR measurement. The presented system is suitable for ultrafast, low-cost, and low-sample volume measurement of ESR at the point-of-care.

Received 16th August 2016,  
Accepted 10th November 2016

DOI: 10.1039/c6lc01036a

www.rsc.org/loc

### Introduction

The erythrocyte sedimentation rate (ESR), discovered in 1897<sup>1</sup> and widely accepted in 1918,<sup>2</sup> is a simple clinical test commonly used as a sickness index for monitoring several inflammatory diseases such as temporal arteritis<sup>3,4</sup> and polymyalgia rheumatica.<sup>5–8</sup> It is also accepted as a critical prognostic factor in some non-inflammatory conditions including stroke,<sup>9</sup> heart attack,<sup>10</sup> and prostate cancer.<sup>11</sup> ESR reflects the rate of settling of erythrocytes in a vertically placed tube filled with whole blood. The erythrocyte-free plasma height at the top of the tube is measured after 30 or 60 min and reported as the ESR value in  $\text{mm h}^{-1}$ . The Westergren method is the gold standard method for ESR measurements, in which a tube with a length of 300 mm and an inner diameter of 2.55 mm is used which requires 5 ml of whole blood sample.<sup>12,13</sup>

Erythrocytes form 3D aggregates that resemble rolls of coins at stasis or at low shear rates in plasma or an appropriate suspending medium.<sup>14–16</sup> This reversible process is the main factor for the non-Newtonian nature of blood, and as such, plays a critical role for blood flow.<sup>17–19</sup> EA is affected by

(i) intrinsic cellular properties (membrane deformability and surface charge density),<sup>20–22</sup> (ii) suspending medium properties (fibrinogen concentration in plasma or aggregation-inducer macromolecule concentration such as dextran),<sup>23–28</sup> and (iii) shear forces on cells.<sup>29–31</sup> EA is of clinical importance for diseases such as sepsis, thrombosis, and circulatory diseases.<sup>16,32,33</sup> Most studies utilize aggregometers that measure EA using photometric methods that quantify the light beam reflected from or transmitted through a blood sample during the aggregation process.<sup>31,34–40</sup> These aggregometers differ from each other based on their mechanical unit, which creates the shear force required for disaggregation. Image analysis of EA under different dynamic conditions and computational analysis have also been employed for the quantification of EA.<sup>41–44</sup> Custom-made optical systems (microscopes and holograms) are also proposed for erythrocyte analysis. These systems carry out non-invasive single cell investigation such as measurement of morphological properties, volume, and refractive index based on interferometric methods.<sup>45–48</sup> Due to the complexities of the optical systems and image retrieval algorithms, these systems are impractical for rapid and facile monitoring and quantification of the fast aggregation process.<sup>49</sup>

Lab-on-a-chip technologies for blood analysis and their commercialization possess significant potential for healthcare.<sup>50,51</sup> There are studies that led to benchtop

<sup>a</sup>Institute of Materials Science and Nanotechnology, National Nanotechnology Research Center (UNAM), Bilkent University, Ankara, 06800, Turkey.  
E-mail: elbuken@unam.bilkent.edu.tr

<sup>b</sup>Yildirim Beyazit University Faculty of Medicine, Ankara, Turkey

commercial products, which measure ESR from aggregation dynamics.<sup>52,53</sup> They work much faster than the Westergren method (~5 min) and use smaller sample volumes (~150  $\mu\text{l}$ ). These products function as photometric rheoscopes,<sup>53</sup> however the detailed working principles of these products are not disclosed. Therefore, it is not possible to evaluate the underlying fundamental phenomena that form the basis of faster ESR measurements claimed in these devices. In this work, we aim at explaining the fundamental relationship between EA and ESR by developing a portable microfluidic system and visualizing the whole disaggregation/aggregation process and correlating it with the corresponding optical transmitted signal.

We measured the rate of EA and used it to predict ESR, leveraging the relationship between particle size and sedimentation rate. Particle sedimentation in a suspending medium is explained by Stokes' law, which states that the sedimentation velocity of a spherical particle is proportional to the square of its radius.<sup>54</sup> EA forms clusters of erythrocytes, which have a higher sedimentation velocity than individual erythrocytes. We explored this direct relationship between erythrocyte aggregates and their settling velocity in order to perform rapid ESR measurements from EA.

Herein, we report a microfluidic system that measures ESR from EA using only 40  $\mu\text{l}$  of whole blood in 2 min. The system consists of a disposable single-channel polycarbonate cartridge and a handheld opto-electro-mechanical analyzer. The test cycle starts off by completely disaggregating erythrocytes in the cartridge using a rigorous back and forth fluid motion generated by a solenoid pinch valve. Then, the fluid motion is ceased, and cells start to aggregate. During this aggregation phase, near infrared light ( $\lambda = 830 \text{ nm}$ ) optically transmitted through the cartridge is measured for 1.5 min. Then, the ESR value is calculated using the optical signal change. For experimental verification of the microfluidic system and the measurement method, whole blood samples of 70 patients were tested with our system. The microfluidic system was shown to correlate with the conventional Westergren method with  $R^2 = 0.86$  using linear regression. This value is higher than the correlation coefficients of commercially available ESR analyzers.<sup>53,55,56</sup> In addition, we integrated a camera to the system and designed a new cartridge including a section for visual observation of the EA process in real-time during ESR measurement. Using this unique cartridge, we were able to demonstrate the one-to-one correspondence between the aggregation of erythrocytes and the optical transmission signal. This microfluidic system is of high value for ultrafast point-of-care ESR measurement, which requires only a drop of whole blood.

## Experimental section

### Materials

For blood samples, ethical approvals were obtained from the Ethics Committee of Yildirim Beyazit University Medical

School, Ankara, Turkey and the Ethics Committee of Bilkent University, Ankara, Turkey. Prior informed consent was taken from the donors involved in the study. For clinical measurement of ESR, whole blood was used without any pre-processing of the blood sample. Therefore, for ESR measurements, 5 ml of fresh venous blood was acquired from 70 volunteers at Yildirim Beyazit University Ankara Ataturk Hospital into vacuum tubes containing ethylenediaminetetraacetic acid (EDTA; 1.5  $\text{mg ml}^{-1}$ ) to prevent coagulation. For visual observation of erythrocytes, pre-processing of whole blood was needed, which consisted of PBS washing, dilution, and dextran addition. Therefore, for EA monitoring, 5 ml of fresh blood was acquired from a healthy male volunteer at Bilkent University Health Center (Ankara, Turkey) into a vacuum tube containing EDTA. The blood was centrifuged three times at 3500 rpm for 4 min, and plasma was replaced with 1 $\times$  phosphate-buffer saline (PBS) solution each time. A microcentrifuge tube was filled with 5  $\mu\text{l}$  of the plasma-free blood sample and 125  $\mu\text{l}$  of PBS and mixed. Then, 1 mg of 150 kDa dextran (Sigma-Aldrich) was added to the tube and dissolved by gentle mixing for 1 min using a pipette.

### Particle sedimentation theory

Stokes' law<sup>54</sup> governs the settling velocity of a spherical particle suspended in a medium, where three forces act on the particle: gravitational ( $F_g$ ), buoyant ( $F_b$ ), and drag ( $F_d$ ) forces. Each can be written as follows:

$$F_g = \rho_{\text{particle}} Vg \quad (1)$$

$$F_b = \rho_{\text{medium}} Vg \quad (2)$$

$$F_d = 6\pi\mu r\mathcal{G} \quad (3)$$

where  $\rho$  is the density,  $V$  is the particle volume,  $g$  is the gravitational acceleration,  $\mu$  is the medium dynamic viscosity,  $r$  is the particle radius, and  $\mathcal{G}$  is the particle settling (termination) velocity. In a stationary system, no other force is effective on the system, thus yielding:

$$F_g = F_b + F_d \quad (4)$$

Plugging eqn (1)–(3) into eqn (4), the particle velocity can be found as follows:

$$\mathcal{G} = \frac{2g}{9} \frac{(\rho_{\text{particle}} - \rho_{\text{medium}})}{\mu} r^2 \quad (5)$$

For non-spherical particles, a correction factor called the dynamic shape factor,  $K$ , is applied to the drag force in eqn (3), yielding:

$$F_d^{\text{non-spherical}} = 6\pi\mu r_e \mathcal{G} K \quad (6)$$

where  $r_e$  is the equivalent volume radius for a spherical particle that has the same volume as the non-spherical particle.<sup>57</sup> By plugging eqn (1), (2) and (6) into eqn (4), the settling velocity valid for non-spherical particles can be found as follows:

$$g = \frac{2g(\rho_{\text{particle}} - \rho_{\text{medium}})}{9\mu K} r_e^2 \quad (7)$$

According to eqn (5) and (7), one can conclude that the sedimentation velocity of a particle in a medium is proportional to the square of the size of the particle.

### Cartridge designs

Disposable cartridges used in this work were fabricated out of polycarbonate (PC), a transparent thermoplastic polymer. Although the use of PDMS microchannels is common in the microfluidic community, we did not use PDMS since it can absorb the blood sample and introduce bias to the optical measurements.<sup>58</sup> The channel designs were made in 2D using CAD software (Autodesk, AutoCAD 2016). The cartridges were manufactured using CNC machining. We had two different cartridge designs. (i) For ESR measurements, cartridge-1 was used, which has a 1 mm deep, 1 mm wide, and 50 mm long channel. (ii) For simultaneous ESR measurement and EA monitoring, cartridge-2 was used, which has a single inlet and outlet and composed of two sections: a deep section ( $h_1 = 1$  mm) for ESR measurement and a shallow section ( $h_2 = 150$   $\mu\text{m}$ ) for EA monitoring.

The relationship between the erythrocyte settling velocity and erythrocyte aggregation is based on the Stokes' law, which is a fundamental equation in fluid mechanics. There are also commercial benchtop instruments that report ESR values within minutes using EA. However, in the literature, there are strong oppositions to the use of these devices, since ensuring complete disaggregation of the erythrocytes is critical for correlating EA and ESR. Therefore, it is of utmost importance to visualize the behavior of erythrocytes during the whole process and correlate it with the optical signal. Cartridge-2 was specifically designed for this purpose. For the optical transmission signal, the system requires a strong interaction between the incident light and the erythrocytes; therefore, the optical path length should be increased using a deep channel. However, monitoring of individual erythrocytes is not possible in a deep microchannel due to the high population of erythrocytes. The visualization system requires a smear-like blood sample. Cartridge-2, which is shown in Fig. 1a, accommodates both of these microchannel segments: a shallow channel for monitoring of individual erythrocytes and a deep channel for optical measurement. However, changing the channel depth changes the wall shear rate as well as the disaggregating force on erythrocytes. Therefore, the width of the shallow channel is increased in order to ensure that the same wall shear rate is experienced in both channel segments as described below.

According to Weissenberg–Rabinowitsch–Mooney equation,<sup>59</sup> the wall shear rate ( $\dot{\gamma}$ ) is calculated as

$$\dot{\gamma} = \frac{6Q}{wh^2} \quad (8)$$

where  $Q$  is the volumetric flow rate,  $w$  is channel width, and  $h$  is channel height. Since volumetric flow rate is the same in the deep and shallow channel segments, the following condition needs to be met for erythrocytes to experience the same disaggregating shear rates in both channel segments in order to satisfy  $\dot{\gamma}_{\text{deep}} = \dot{\gamma}_{\text{shallow}}$

$$w_{\text{deep}}h_{\text{deep}}^2 = w_{\text{shallow}}h_{\text{shallow}}^2 \quad (9)$$

The channel heights were set as  $h_{\text{deep}} = 1$  mm and  $h_{\text{shallow}} = 150$   $\mu\text{m}$ . The widths for both sections were set as  $w_{\text{deep}} = 1$  mm and  $w_{\text{shallow}} = 44.5$  mm, satisfying eqn (9). The lengths were chosen as  $L_{\text{deep}} = 50$  mm, and  $L_{\text{shallow}} = 7.5$  mm. The length of the deep channel segment (50 mm) is the same as the length of cartridge-1.

### Microfluidic measurement system

We developed a microfluidic measurement system that optically measures the rate of EA and calculates ESR from EA. Fig. 1a shows the schematic representation of the whole system that contains a disposable polycarbonate cartridge and a handheld analyzer. Two different cartridges were designed for the experiments. An acrylic cartridge holder was also fabricated in which the cartridges are secured tightly to prevent any vibration during the measurements. The holder also contains a tygon tubing system, one end of which seals the cartridge outlet port when the cartridge is inserted to the holder. Cartridge-1, which contains a deep single channel (1 mm wide, 1 mm high), was fabricated for the optical measurement of ESR, since a dense population of erythrocytes was required for stronger interaction of the cells with the incident light in order to obtain satisfactory signal change on the photodetector. Cartridge-2 consists of deep (1 mm wide, 1 mm high) and shallow (44.5 mm wide, 150  $\mu\text{m}$  high) sections; the latter was designed for real-time observation of the erythrocytes during the whole test cycle. The opto-electromechanical analyzer which is shown in Fig. 1b consists of three units: (i) a mixing unit, (ii) an optical unit, and (iii) an electronic control unit. For the mixing unit, a solenoid pinch valve (EW-98302-02, Cole-Parmer) is employed to provide continuous rigorous back and forth blood sample movement in the cartridge for 15 s. The pinch valve stroke distance (5 mm) is adjusted so that the shear rate applied by the valve on the erythrocytes is above the critical shear rate ( $\dot{\gamma}_{\text{critical}}$ ) for complete erythrocyte disaggregation. The measurement principle of the system is based on the analysis of optically transmitted light through the blood sample which is schematically shown in Fig. 1c. In the optical unit, a near infrared (NIR) light-emitting diode (LED) with an 830 nm wavelength and a NIR

photodetector are employed. The NIR band is chosen to minimize the absorption of light by the erythrocytes,<sup>16</sup> which in turn increases the light scattering from and transmission through the blood sample.<sup>60</sup> The LED (VSMG2700, Vishay) is placed at the top surface of the cartridge and illuminates the blood-filled channel. Light that passes through the channel is collected on the photodetector (VEMT4700, Vishay) located at the bottom of the cartridge. In the electronic control unit, a custom-designed electronic circuitry and a microprocessor (IOIO-OTG, SparkFun) are used. The electronic circuitry controls the pumping action and the optical unit. The former circuit is a single transistor (BD139 NPN, STMicroelectronics) employed as a switch and controlled by the microcontroller such that the solenoid valve is activated 15 times during the 15 s disaggregation phase. The detection circuit consists of a transimpedance amplifier connected to the phototransistor output, followed by a low-pass filter. The system is controlled through a computer user interface that can be used to adjust the intensity of LED, mixing time, and total analysis time.

Cartridge-1 takes 40  $\mu\text{l}$  of a whole blood sample, and cartridge-2 takes 200  $\mu\text{l}$  of a pre-processed blood sample. Upon the sample introduction into the cartridge, the test cy-

cle was started by completely disaggregating the erythrocytes for 15 s using the pinch valve. Then, the valve was turned off, allowing the cells to re-aggregate. During the aggregation process, the sample was illuminated with the LED, and transmitted light was measured by the photodetector. Within the channel, each individual erythrocyte acts as a scattering center.<sup>16,48</sup> Since the individual erythrocyte population is high, the intensity level is at its lowest when the cells are completely disaggregated (Fig. 1c). On the other hand, the intensity level reaches its maximum at complete aggregation. Between the min and max values, as cells aggregate, the intensity level increases. The transmitted signal was recorded for 90 s. The amplitude of the transmitted signal, which is the difference between the signal level at the 90th s and the signal level at the start of the aggregation process, was calculated using Matlab (R2014, MathWorks) and recorded as the aggregation index (AI). The results are verified using the measurements performed using the conventional Westergren method shown in Fig. 1d. For real-time observation of the EA process, the shallow section is monitored using a 40 $\times$  microscope objective (Axio Vert.A1, Zeiss) coupled to a camera (Axiocam ICc 1, Zeiss).

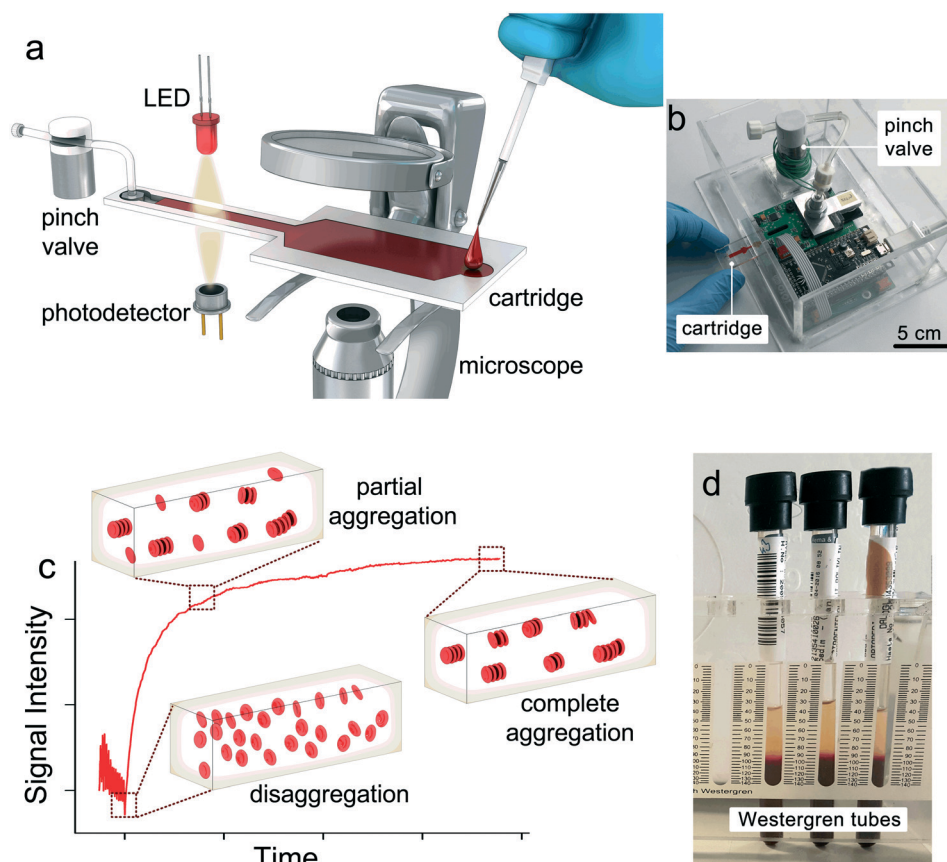


**Fig. 1** The microfluidic system for ultrafast ESR measurement and EA monitoring. (a) Schematic representation of the system and the method. A pinch valve disaggregates erythrocytes in whole blood, and a photodetector collects optically transmitted light for ESR measurement. An optical microscope and a camera set-up allow real-time monitoring of the aggregation process. (b) The hand-held and portable microfluidic system developed for ESR measurement at the point-of-care. (c) Typical transmitted signal intensity *versus* time curve obtained from the microfluidic system during ESR measurement. The minimum intensity corresponds to complete disaggregation and the maximum intensity corresponds to complete aggregation. Between these intervals, aggregation occurs. (d) The Westergren method which is used for conventional ESR measurements.

## Results and discussion

### Quantifying the aggregation of erythrocytes

The microfluidic system records optically transmitted light through the blood sample. The minimum intensity of light indicates complete disaggregation of the cells. During the aggregation process, the intensity level increases as shown in Fig. 2. To quantify the aggregation of erythrocytes, two aggregation indices ( $AI_1$  and  $AI_2$ ) were calculated.  $AI_1$  is the area under the curve ( $A$ ) divided by the total area ( $A + B$ ) of the transmitted signal, whereas  $AI_2$  is the amplitude (AMP) that corresponds to the change of the transmitted signal.<sup>16</sup> The total analysis time is another parameter to be considered. We have calculated  $AI_1$  and  $AI_2$  for a series of analysis durations from 30 s to 120 s. Fig. 2a shows the transmitted signal intensities of four whole blood samples with different ESR values (11 mm h<sup>-1</sup>, 16 mm h<sup>-1</sup>, 33 mm h<sup>-1</sup>, and 54 mm h<sup>-1</sup>) measured using the Westergren method. The samples were chosen such that two samples were in the normal ESR range (0 mm h<sup>-1</sup> ≤ ESR ≤ 30 mm h<sup>-1</sup>), and the other two were in the clinical ESR range (ESR > 30 mm h<sup>-1</sup>). The signals were recorded for 120 s after complete disaggregation. For each test, the two aggregation indices were calculated for different assay times (30, 36, 42, ... 120 s). Using the two aggregation indices defined above, in total, 32 AI values were calculated. Then, for each of the 32 AIs, the parity plot was obtained using the ESR values measured by the 30 min Westergren method ( $W_{30}$ ) and the AI of interest. For each curve, the goodness of the fit ( $R^2$ ) was calculated. Fig. 2b and c give the goodness of fit of  $AI_1$  and  $AI_2$ , respectively, measured for different analysis durations. As seen in Fig. 2,  $R^2$  for  $AI_1$  differs significantly for different test durations whereas  $R^2$  for  $AI_2$  is consistent and has a value closer to 1 at all assay times.

### ESR measurement with the microfluidic system

After determining the aggregation index that has the highest correlation with the conventional ESR method, whole blood samples of 70 volunteers were tested with the microfluidic system and compared with the measurements obtained by the gold standard method. Attention was paid in order to span a wide dynamic range covering both the healthy and clinical ESR ranges. The ESR values of the samples were first measured using the automated ESR analyzer (Linear Chemicals, Autoanalyzer) employing the 30 min Westergren ESR method within 1 h of venipuncture. Upon the measurement with the analyzer, 40 μl of whole blood was withdrawn from each Westergren tube and tested with the microfluidic system at room temperature (24 °C).  $AI_2$  measured at the 90th s was chosen as the basis for the microfluidic ESR method. This value was calculated from the transmitted signal intensity of each volunteer sample. The regression analysis of the measurements is shown in Fig. 3, where the y-axis is the conventionally measured ESR values of the 70 volunteers, and the x-axis is the calculated aggregation indices corresponding to each sample's optical transmission signal as shown in Fig. 3. The overall correlation coefficient ( $R^2$ ) of the regression curve is 0.86. The correlation coefficient ( $R^2$ ) is 0.79 in the normal ESR range (0 mm h<sup>-1</sup> ≤ ESR ≤ 30 mm h<sup>-1</sup>), whereas it is 0.69 in the clinical ESR range (ESR > 30 mm h<sup>-1</sup>).

In the clinical setting, the ESR value of 30 mm h<sup>-1</sup> is accepted as the cut-off for further investigation of infection.<sup>8,12,33</sup> Therefore, we analysed our results both in the whole dynamic range and also in the healthy and clinical ranges. The correlation coefficient value in the normal ESR range (0–30 mm h<sup>-1</sup>) is higher than that in the clinical ESR

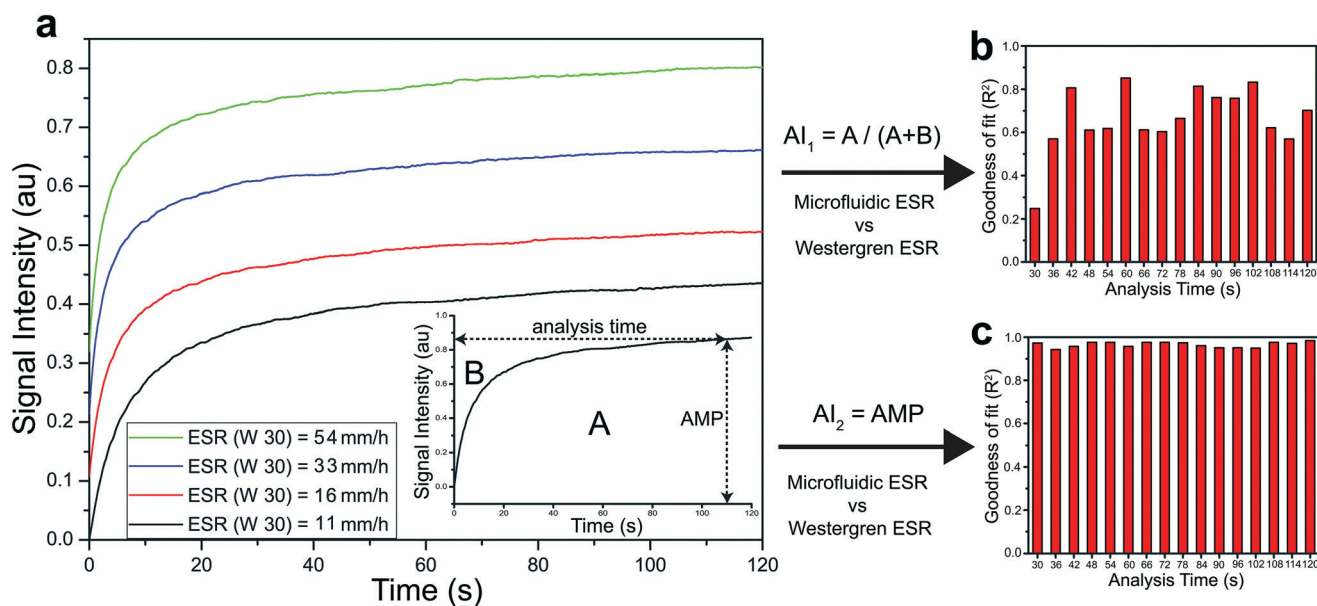
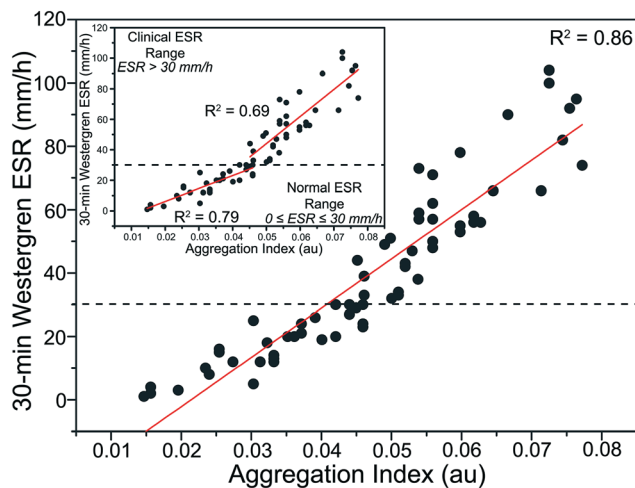


Fig. 2 Aggregation indices calculated for the ESR measurement.  $n = 4$  whole blood samples were tested using an Westergren ESR analyzer as reference. (a) Transmitted signal intensity of the 4 samples recorded for 120 s using the microfluidic system. Goodness of fit,  $R^2$ , between the Westergren ESR and microfluidic ESR for (b)  $AI_1$  and (c)  $AI_2$  measured at increasing analysis times.



**Fig. 3** Comparison of the microfluidic system test results with the gold standard Westergren method.  $n = 70$  whole blood samples tested using the Westergren ESR analyzer (y-axis) and the microfluidic system (x-axis). Goodness of fit,  $R^2$ , is 0.86 using linear regression analysis. Inset:  $n = 35$  blood samples in the normal ESR range ( $0 \leq \text{ESR} \leq 30 \text{ mm h}^{-1}$ ),  $R^2$  of 0.79;  $n = 35$  blood samples in the clinical ESR range ( $>30 \text{ mm h}^{-1}$ ),  $R^2$  of 0.69.

range ( $>30 \text{ mm h}^{-1}$ ). Although the correlation is weakened at high ESR values, it does not pose a problem for the microfluidic ESR system; since quantitative analysis is not required for high ESR values in clinics. It suffices to identify the patients with high ESR values who are directed to specialists for further analysis.

### Precision and repeatability

After finding the linear equations that are used to calculate ESR values from the  $\text{AI}_2$  measurements, the performance of the microfluidic system was further evaluated. First, the precision of the microfluidic system was tested. For the precision tests, whole blood samples of 5 volunteers were first measured with the Westergren method as 4, 21, 33, 54, and  $100 \text{ mm h}^{-1}$  (Fig. 4, x-axis). Following the conventional measurements using the Westergren analyzer, each sample was tested five times with the microfluidic system. The mean values were 4, 21, 36, 46, and  $78 \text{ mm h}^{-1}$ , respectively (Fig. 4, y-axis). The standard deviation for each sample was calculated as 0.82, 0, 1.41, 5.03, and  $1.64 \text{ mm h}^{-1}$ , respectively, and shown as error bars in Fig. 4.

The measurements for the precision tests (Fig. 4) were repeated immediately one after the other, determining how precise the measurements were within a very short period of time. It is also important to look at the device performance when there is a delay between the repetitive measurements. Clinically, this is a significant concern, since the time gap between the blood sampling from the patient and testing in a central laboratory varies from a few minutes to 4–5 hours. This time gap shows variability not only between different health centers but also within the same center. Therefore, it is critical to test the repeatability of the system for samples

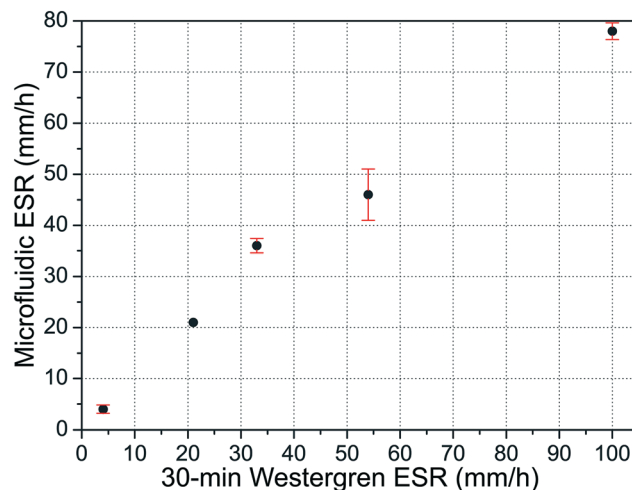


**Fig. 4** Precision tests for the microfluidic system.  $n = 5$  whole blood samples tested. Samples were first tested with the Westergren ESR analyzer (x-axis), and five times with the microfluidic system (y-axis). Error bars denote 2 standard deviations (SD).

stored in blood sampling tubes for different times. For these repeatability tests, two whole blood samples were chosen with ESR values of  $30 \text{ mm h}^{-1}$  and  $57 \text{ mm h}^{-1}$  (W 30). The samples were tested four times using the microfluidic system over the course of 3 h, with 1 h delay between measurements. As shown in Fig. 5b, for the sample with an ESR value of  $30 \text{ mm h}^{-1}$ , the mean and the standard deviation of the four measurements were  $27.3 \text{ mm h}^{-1}$  and  $1.3 \text{ mm h}^{-1}$ , respectively. For the  $57 \text{ mm h}^{-1}$  ESR sample, the mean and the standard deviation were  $52 \text{ mm h}^{-1}$  and  $2.9 \text{ mm h}^{-1}$ , respectively. These results demonstrate that aggregation dynamics of the erythrocytes are not affected with the 3 h storage of the sample at room temperature.

### Simultaneous ESR measurement and EA monitoring

Another major goal of this study is to demonstrate the correspondence between the erythrocyte aggregation dynamics and the optical transmission signal obtained from the portable microfluidic system. Fig. 6 shows the transmitted signal intensity for the pre-processed blood sample filled within cartridge-2. The intensity–time curve includes both the disaggregation phase (lasting for 15 s) and the aggregation phase (lasting for 6 min). The blood sample was diluted (plasma-free and suspended in PBS) to observe individual cells in the shallow section. Then, 150 kDa dextran was added to induce cell aggregation. Cartridge-2 was uniquely designed such that (i) the cells in the shallow section can be monitored under a microscope, (ii) the diluted sample gives satisfactory optical transmission in the deep section, and (iii) the disaggregating shear rates on the cells in both cartridge sections are the same (see the Microfluidic measurement system section). 200  $\mu\text{l}$  of the prepared blood sample was introduced into the cartridge. After rigorous mixing of the sample, which achieves complete disaggregation as shown in Fig. 6 at time: 0 min,

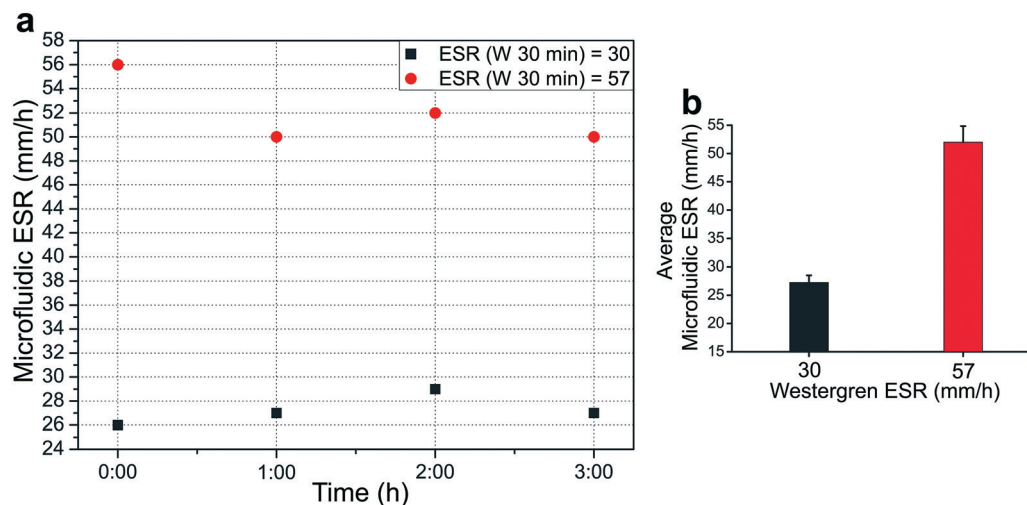


**Fig. 5** Repeatability performance of the microfluidic system. (a)  $n = 2$  whole blood samples with the ESR (W 30 min) values of  $30 \text{ mm h}^{-1}$  (black square) and  $57 \text{ mm h}^{-1}$  (red circle) tested with the microfluidic system. Samples were first tested with the Westergren ESR analyzer, and then four times with the microfluidic system with 1 h delay between consecutive tests. (b) The mean ( $27.25 \text{ mm h}^{-1}$ ) and SD ( $1.26 \text{ mm h}^{-1}$ ) for the sample with ESR of  $30 \text{ mm h}^{-1}$  and the mean ( $52 \text{ mm h}^{-1}$ ) and SD ( $2.83 \text{ mm h}^{-1}$ ) for the sample with ESR of  $57 \text{ mm h}^{-1}$ .

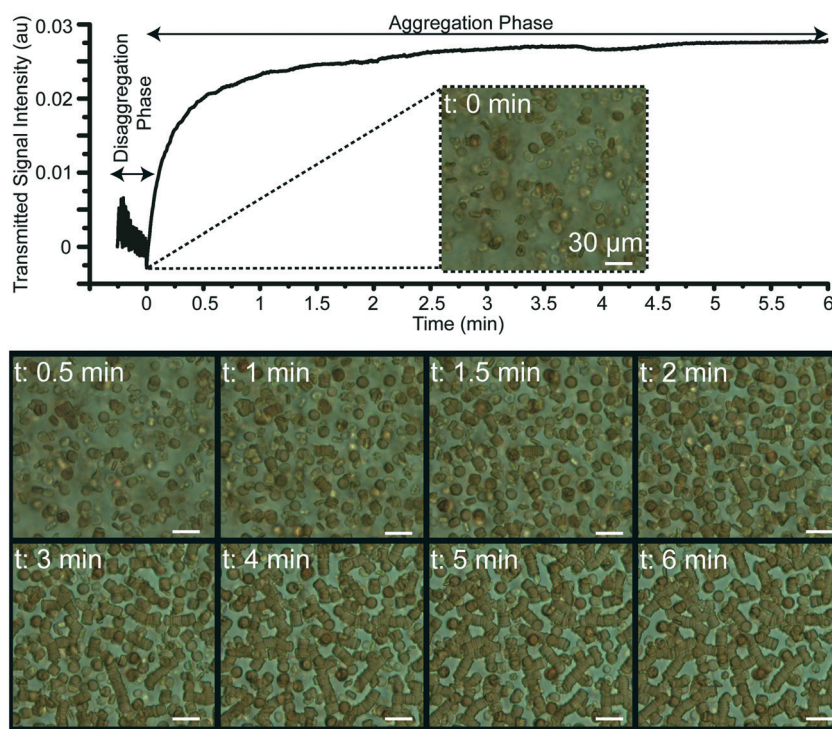


**Fig. 6** Simultaneous ESR measurement and EA monitoring with the microfluidic system.  $200 \mu\text{l}$  of a pre-processed blood sample was filled into cartridge-2 and optical measurement taken from the deep section for 6 min after complete disaggregation. The erythrocyte aggregation process was monitored in the shallow section for 6 min simultaneously as the ESR measurement. A plot showing the transmitted signal intensity measured for 6 min, and the time-lapse images of the aggregation process starting with complete disaggregation ( $t: 0 \text{ min}$ ).

the cells were left intact for 6 min. During that time, the optically transmitted signal was measured in the deep section, and the erythrocyte aggregation process was video-recorded at the same time. In addition to the intensity–time curve, Fig. 6 gives time-lapse images taken from the recorded video. The time at which each image was taken has one-to-one correspondence with the intensity–time curve. At time: 0 min,

the mixing was stopped, and the transmitted signal intensity was at its minimum when the cells were completely disaggregated. As time proceeded, the cells were shown to aggregate. At the beginning, aggregation was rapid and erythrocytes form bridges with the neighbouring cells. At time: 3 min, even though there are individual cells, most of the cells were clustered as aggregates. After time: 3 min, aggregates

proceeded at a much lower rate which is also confirmed by the intensity–time curve.

Although there are some studies in the literature that discuss the correlation between erythrocyte aggregation and sedimentation, none of these studies show the process in real-time. Also, a drawback of the commercial devices in the market is their potential incapability for succeeding complete disaggregation at the beginning of the assay.<sup>55,61</sup> The microscopy observations we made using cartridge-2 explains the correlation between erythrocyte aggregation and light intensity change. At complete disaggregation, each cell becomes a scattering center,<sup>16</sup> and their collective scattering results in less signal transmitting through the blood sample, leading to the lowest transmission intensity. During the aggregation phase, the total area of the scattering centers decreases. This leads to more light passing through the microchannel, resulting in an increase of the transmitted signal intensity.

In whole blood, erythrocytes cannot be thought of as independent from the other blood constituents. There are many internal factors that affect the rate of erythrocyte sedimentation measured by the Westergren method. These include the hematocrit level, plasma protein concentration, erythrocyte deformability, temperature, plasma viscosity and density.<sup>16,55,61,62</sup> Some of these factors affecting the sedimentation might not affect the aggregation dynamics. For example, plasma viscosity has a major effect on the settling time of erythrocytes in the conventional system, but it has a minor effect in our system due to the fast measurement of the aggregation mechanism in a very small region of the cartridge. In contrast, erythrocyte deformability has a relatively minor effect in the conventional system, but it changes the aggregability of erythrocytes resulting in a major effect in our system. Since the microfluidic system that we developed measures the rate of EA and use it to predict ESR, some of these factors might be under or overestimated. This also explains the correlation coefficient of  $R^2 = 0.86$ .

On the other hand, there are several external factors influencing ESR results obtained by the Westergren method. These include (i) the initial sample volume in the tube, (ii) tube vertical positioning, (iii) vibration, (iv) homogeneity of the sample at the beginning of the assay, (v) delay between venipuncture and measurement, and (vi) manual reading of the result by the operator. Our portable microfluidic system addresses all of these shortcomings of the conventional method. (i) Measurement is performed at a single point along the sample channel. Cartridge-1 requires 40  $\mu\text{l}$  of a sample to fill the channel. Deviation from this amount does not affect the results as long as there is sample in front of the sensor during the test. (ii) Erythrocyte aggregation is not affected by the cartridge/analyzer orientation. (iii) The system is vibration-proof; carrying the system in hand during the measurement does not affect the results. (iv) Homogeneity of the sample and complete disaggregation were ensured by sample mixing at the beginning of the test cycle. However, in the conventional assay, the operator should ensure sample homogeneity before placing the tube into the analyzer. (v)

Since the system is portable and requires a very small sample volume, the measurement can be carried out at the point-of-care without any delay. (vi) The system is a truly sample-in result-out system, thus eliminates operator mistakes.

## Conclusion

We have developed a portable microfluidic system that determines the erythrocyte sedimentation rate (ESR) from erythrocyte aggregation (EA). We experimentally showed the correlation between the two physiological phenomena. We explained the fundamental relationship between ESR and EA using Stokes' law. Erythrocyte aggregates of large cell clusters lead to a higher sedimentation velocity. This direct relationship was used for rapid measurement of ESR. The microfluidic system uses 40  $\mu\text{l}$  of whole blood and completes the test in 2 min. We measured the aggregation index from the transmitted signal passing through the sample, which relates ESR to EA. The results were compared with the conventional Westergren method and the microfluidic system showed high repeatability. We also showed the real-time observation of erythrocytes during ESR measurement using a unique cartridge geometry. Simultaneous ESR measurement and EA monitoring demonstrated one-to-one correspondence between the optical signal and the erythrocyte disaggregation and aggregation phases. The system was shown to eliminate the drawbacks of the Westergren method (operator-related problems such as tube shaking, sample volume, tube positioning, and result reading). The presented microfluidic system is a low sample volume requiring, low-cost, and portable system for ultrafast ESR measurement that can be used at point-of-care.

## Acknowledgements

The authors acknowledge support from The Scientific and Technological Research Council of Turkey (TUBITAK project no. 213S127).

## References

- 1 A. Grzybowski and J. Sak, *Clin. Dermatol.*, 2011, **29**, 697–703.
- 2 A. L. F. Westergren, *Acta Med. Scand.*, 1921, **54**, 247–282.
- 3 M. R. Cheema and S. M. Ismaeel, *Clin. Interventions Aging*, 2016, **11**, 185–188.
- 4 R. L. Wong and J. H. Korn, *Am. J. Med.*, 1986, **80**, 959–964.
- 5 J. H. C. Sox and M. H. Liang, *Ann. Intern. Med.*, 1986, **104**, 515–523.
- 6 F. Wolfe and K. Michaud, *J. Rheumatol.*, 1994, **21**, 1227–1237.
- 7 S. M. Helfgott and R. I. Kieval, *Arthritis Rheum.*, 1996, **39**, 304–307.
- 8 M. Plebani and E. Piva, *Am. J. Clin. Pathol.*, 2002, **117**, 621–626.
- 9 A. S. Singh, V. Atam, B. E. Yathish, L. Das and S. Koonwar, *J. Neurosci. Rural Pract.*, 2014, **5**, 40–45.
- 10 M. B. Andresdottir, N. Sigfusson, H. Sigvaldason and V. Gudnason, *Am. J. Epidemiol.*, 2003, **158**, 844–851.

- 11 J.-E. Johansson, T. Sigurdsson, L. Holmberg and R. Bergstrom, *Cancer*, 1992, **70**, 1556–1563.
- 12 S. E. Bedell and B. T. Bush, *Am. J. Med.*, 1985, **78**, 1001–1009.
- 13 B. S. Bull, M. Caswell, E. Ernst, J. M. Jou, A. Kallner, J. A. Koepke, S. M. Lewis, G. D. O. Lowe, M. W. Rampling and J. Stuart, *J. Clin. Pathol.*, 1993, **46**, 198–203.
- 14 D. Brooks, in *Blood Cells, Rheology, and Aging*, Springer, 1988, pp. 158–162.
- 15 B. Neu and H. J. Meiselman, *Handbook of Hemorheology and Hemodynamics*, 2007, vol. 69, p. 114.
- 16 O. Baskurt, B. Neu and H. J. Meiselman, *Red blood cell aggregation*, CRC Press, 2011.
- 17 H. Amini, W. Lee and D. Di Carlo, *Lab Chip*, 2014, **14**, 2739–2761.
- 18 S. Chien, *The red blood cell*, 1975, vol. 2, pp. 1031–1133.
- 19 G. Tomaiuolo, M. Barra, V. Preziosi, A. Cassinese, B. Rotoli and S. Guido, *Lab Chip*, 2011, **11**, 449–454.
- 20 K.-M. Jan and S. Chien, *J. Gen. Physiol.*, 1973, **61**, 638–654.
- 21 G. Nash and H. Meiselman, *Biorheology*, 1984, **22**, 73–84.
- 22 M. Rampling, H. Meiselman, B. Neu and O. Baskurt, *Biorheology*, 2004, **41**, 91–112.
- 23 N. Maeda, K. Imaizumi, M. Sekiya and T. Shiga, *Biochim. Biophys. Acta, Biomembr.*, 1984, **776**, 151–158.
- 24 N. Maeda and T. Shiga, *Biochim. Biophys. Acta, Gen. Subj.*, 1985, **843**, 128–136.
- 25 M. Boynard and J. Lelievre, *Biorheology*, 1989, **27**, 39–46.
- 26 N. Maeda, M. Seike, T. Nakajima, Y. Izumida, M. Sekiya and T. Shiga, *Biochim. Biophys. Acta, Biomembr.*, 1990, **1022**, 72–78.
- 27 G. Barshtein, I. Tamir and S. Yedgar, *Eur. Biophys. J.*, 1998, **27**, 177–181.
- 28 B. Neu, R. Wenby and H. J. Meiselman, *Biophys. J.*, 2008, **95**, 3059–3065.
- 29 S. Shin, J.-H. Nam, J.-X. Hou and J.-S. Suh, *Clin. Hemorheol. Microcirc.*, 2009, **42**, 117–125.
- 30 H.-J. Lim, Y.-J. Lee, J.-H. Nam, S. Chung and S. Shin, *J. Biomech.*, 2010, **43**, 546–550.
- 31 O. K. Baskurt, M. Uyklu, S. Ozdem and H. J. Meiselman, *Clin. Hemorheol. Microcirc.*, 2011, **47**, 295–305.
- 32 O. K. Baskurt, A. Temiz and H. J. Meiselman, *J. Lab. Clin. Med.*, 1997, **130**, 183–190.
- 33 O. K. Baskurt and H. J. Meiselman, *Clin. Hemorheol. Microcirc.*, 2013, **53**, 23–37.
- 34 B. S. Bull and J. D. Brailsford, *Blood*, 1972, **40**, 550–559.
- 35 D. Pieragalli, S. Forconi, M. Guerrini, A. Acciavatti, C. Galigani, C. Del Bigo and T. Di Perri, *Ric. Clin. Lab.*, 1984, **15**, 79–86.
- 36 O. K. Baskurt, H. Meiselman and E. Kayar, *Clin. Hemorheol. Microcirc.*, 1998, **19**, 307–314.
- 37 M. Hardeman, J. Dobbe and C. Ince, *Clin. Hemorheol. Microcirc.*, 2001, **25**, 1–11.
- 38 O. K. Baskurt, M. Uyklu, M. R. Hardeman and H. J. Meiselman, *J. Biomed. Opt.*, 2009, **14**, 054044.
- 39 O. K. Baskurt, M. Uyklu, P. Ulker, M. Cengiz, N. Nemeth, T. Alexy, S. Shin, M. R. Hardeman and H. J. Meiselman, *Clin. Hemorheol. Microcirc.*, 2009, **43**, 283–298.
- 40 E. Hysi, R. K. Saha and M. C. Kolios, *Biomed. Opt. Express*, 2012, **3**, 2326–2338.
- 41 S. Chen, G. Barshtein, B. Gavish, Y. Mahler and S. Yedgar, *Clin. Hemorheol. Microcirc.*, 1994, **14**, 497–508.
- 42 S. Chen, B. Gavish, S. Zhang, Y. Mahler and S. Yedgar, *Biorheology*, 1995, **32**, 487–496.
- 43 G. Barshtein, D. Wajnbblum and S. Yedgar, *Biophys. J.*, 2000, **78**, 2470–2474.
- 44 S. Jayavanth and M. Singh, *ITBM-RBM*, 2004, **25**, 67–74.
- 45 B. Rappaz, P. Marquet, E. Cuche, Y. Emery, C. Depeursinge and P. Magistretti, *Opt. Express*, 2005, **13**, 9361–9373.
- 46 S. Mavandadi, S. Feng, F. Yu, S. Dimitrov, K. Nielsen-Saines, W. R. Prescott and A. Ozcan, *PLoS One*, 2012, **7**, e46192.
- 47 T. Kim, R. Zhou, M. Mir, S. D. Babacan, P. S. Carney, L. L. Goddard and G. Popescu, *Nat. Photonics*, 2014, **8**, 256–263.
- 48 D. Dannhauser, D. Rossi, F. Causa, P. Memmolo, A. Finizio, T. Wriedt, J. Hellmers, Y. Eremin, P. Ferraro and P. Netti, *Lab Chip*, 2015, **15**, 3278–3285.
- 49 L. Miccio, P. Memmolo, F. Merola, P. A. Netti and P. Ferraro, *Nat. Commun.*, 2015, **6**, 6502.
- 50 C. D. Chin, V. Linder and S. K. Sia, *Lab Chip*, 2012, **12**, 2118–2134.
- 51 C. van Berkel, J. D. Gwyer, S. Deane, N. Green, J. Holloway, V. Hollis and H. Morgan, *Lab Chip*, 2011, **11**, 1249–1255.
- 52 M. Plebani, S. De Toni, M. C. Sanzari, D. Bernardi and E. Stockreiter, *Am. J. Clin. Pathol.*, 1998, **110**, 334–340.
- 53 N. Boğdaycıoğlu, F. M. Yilmaz, S. Sezer and E. Oğuz, *J. Clin. Lab. Anal.*, 2015, **29**, 397–404.
- 54 G. G. Stokes, *On the effect of the internal friction of fluids on the motion of pendulums*, Pitt Press, 1851.
- 55 M. R. Hardeman, M. Levitus, A. Pelliccia and A. A. Bouman, *Scand. J. Clin. Lab. Invest.*, 2010, **70**, 21–25.
- 56 J. Curvers, J. Kooren, M. Laan, E. van Lierop, D. Van de Kerkhof, V. Scharnhorst and M. Herruer, *Am. J. Clin. Pathol.*, 2010, **134**, 653–660.
- 57 W. C. Hinds, *Aerosol technology: properties, behavior, and measurement of airborne particles*, John Wiley & Sons, 2012.
- 58 E. Berthier, E. W. Young and D. Beebe, *Lab Chip*, 2012, **12**, 1224–1237.
- 59 C. Macosko, *Rheology: Principles, Measurements, and Applications*, Wiley-VCH, New York, 1994.
- 60 M. Li, D. N. Ku and C. R. Forest, *Lab Chip*, 2012, **12**, 1355–1362.
- 61 M. R. Hardeman, M. Levitus, A. Pelliccia and A. A. Bouman, *Scand. J. Clin. Lab. Invest.*, 2010, **70**, 26–32.
- 62 Y. Zheng, J. Nguyen, Y. Wei and Y. Sun, *Lab Chip*, 2013, **13**, 2464–2483.